

TECHNICAL UNIVERSITY OF CRETE  
ELECTRICAL AND COMPUTER ENGINEERING DEPARTMENT  
TELECOMMUNICATIONS DIVISION



**Passive radar with ambient illuminators and  
low-cost software-defined radios.**

by

Iosif Vardakis

A THESIS SUBMITTED IN PARTIAL FULFILLMENT OF  
THE REQUIREMENTS FOR THE DIPLOMA OF  
ELECTRICAL AND COMPUTER ENGINEERING

July 2020

THESIS COMMITTEE

Professor Aggelos Bletsas, *Thesis Supervisor*  
Professor George N. Karystinos  
Professor Michalis E. Zervakis

# Abstract

This thesis presents a complete implementation of a low-cost FM passive radar. The hardware and software of the setup are explained in detail, including the low-cost, 12-bit resolution LimeSDR USB receiver. The adaptive filters Least-Squares (LS), Normalized Least-Mean-Square (NLMS), Block NLMS (BNLMS) and Fast BNLMS (FBNLMS) were implemented. Their effectiveness on suppressing the clutter reflections and their runtimes are compared. The results show that the fastest algorithm is FBNLMS, achieving the clutter removal processing in 0.7 seconds with a standard laptop computer. This is less than the Coherent Processing Interval (CPI), chosen at 1.09 seconds and sampling rate of 2.4 Msamples per second. As a result, it is the best choice for a real-time passive radar. NLMS had the best performance in terms of clutter removal, reducing the noise floor 6.2 dB compared to FBNLMS and 4.9 dB compared to LS. The LS filter proved to be a good trade-off between time efficiency and clutter suppression. In addition, an efficient algorithm to compute the cross-ambiguity function, along with a simple constant false alarm rate for target detection are included. Experimental results calculating the accuracy of the passive radar in both bistatic range and Doppler frequency are presented. The commercial flight OAL5SA that departed from the airport of Chania in the 14th of July, 2020, was used to measure the theoretical bistatic range and Doppler frequency, with a publicly available flight tracking application. Comparing the experimental outcomes with the theoretic measurements showed that in the bistatic range, there is an average error of 2795 metres and in the Doppler frequency there is an average error of 7 Hz.

# Acknowledgements

First of all, I would like to thank my supervisor Prof. Aggelos Bletsas for giving me the opportunity to work on such an exciting project and for all his support throughout this work.

Second of all, I would like to offer my special thanks to Georgios Vougioukas and Max Manning for their invaluable help. Also, I am extremely grateful to my colleagues Vaggelis Giannelos, Konstantinos Skyvalakis, Manos Andrianakis and Vaggelis Karatarakis.

Of course, I would like to acknowledge the priceless support provided by my family during my studies. My close friends and colleagues Giorgos Apostolakis, Manolis Pagkalos, Giannis Karvounakis and Roza Chatzigeorgiou, with whom we share great memories from those 5 years of knowing each other and studying together.

# Table of Contents

<b>Table of Contents</b> . . . . .	4
<b>List of Figures</b> . . . . .	6
<b>1 Introduction</b> . . . . .	8
<b>2 System overview</b> . . . . .	11
2.1 Software Overview . . . . .	12
2.2 Hardware . . . . .	13
2.2.1 Antennas . . . . .	13
2.2.2 SDR . . . . .	15
<b>3 Clutter removal</b> . . . . .	17
3.1 Continuous-time model . . . . .	17
3.2 Discrete-time model . . . . .	19
3.3 Adaptive filters . . . . .	21
3.3.1 Least-Squares . . . . .	22
3.3.2 Least-Mean-Square . . . . .	24
3.3.3 Normalized Least-Mean-Square . . . . .	27
3.3.4 Block Normalised Least-Mean-Square . . . . .	27
3.3.5 Fast Block Normalised Least-Mean-Square . . . . .	28
<b>4 ARD Surface plot</b> . . . . .	32
4.1 Cross-ambiguity function . . . . .	32
4.2 Constant False Alarm Rate . . . . .	34
<b>5 Experimental results</b> . . . . .	36
5.1 Adaptive Filters' performance . . . . .	36
5.2 Range-Doppler accuracy . . . . .	40
<b>6 Conclusions</b> . . . . .	44

---

**Bibliography** . . . . . 45

# List of Figures

1.1	The FM station in Malaxa and the PR setup. . . . .	9
2.1	Representation of the FM signals captured by a passive radar . . . . .	11
2.2	Stages of the PR processing. . . . .	12
2.3	The reference antenna and the FM Station on the opposing mountain in the area of Malaxa. . . . .	13
2.4	The observation antenna. . . . .	14
2.5	The two RTL-SDRs with the connected clock. . . . .	15
2.6	A LimeSDR-USB used for receiving the Reference and Observation signals. . . . .	16
3.1	The adaptive filter's generalized structure for interference cancellation.	21
3.2	Model of the linear transversal filter with the $\hat{w}$ . . . . .	23
3.3	The transversal filter of the LMS algorithm. . . . .	26
3.4	A schematic representation of the FBNLMS algorithm. . . . .	31
4.1	"Fine mode" cross-ambiguity computation for faster calculation of $\psi(\tau, f)$ . . . . .	34
4.2	CFAR kernel: Cell Under Test(CUT) with red, Guard cells with blue, Reference cells with green and the rest of the frame in white(Data window). . . . .	35
4.3	Without CFAR. . . . .	35
4.4	With CA-CFAR. . . . .	35
5.1	Unfiltered picture. . . . .	38
5.2	Least-Squares filter. . . . .	39
5.3	NLMS filter. . . . .	39
5.4	FBNLMS filter. . . . .	40
5.5	Tracking application information. . . . .	41
5.6	Coordinates of the plane during flight OAL5SA, according to tracking app. . . . .	41

---

5.7	The bistatic radar geometry. . . . .	42
5.8	Doppler measurements of the radar versus the theoretical. . . . .	43
5.9	Range measurements of the radar versus the theoretical. . . . .	43

# Chapter 1

## Introduction

Radar is a detection system using radio waves to determine the range, angle or velocity of targets. A transmitter sends radio waves, which contact the target and a fraction of them is reflected towards the receiver. In a bistatic passive radar (PR), signals are emitted by illuminators of opportunity, such as FM radio stations or DVB-T stations and the reflections along with the direct signal are captured by receivers away from those stations.

Passive radars are an interesting research field. They have certain advantages over classic active monostatic radars, which have their own dedicated transmitter placed at the same location with the receiver. Some of the attractive features of a PR, according to [1], [2] are listed below:

- It enables utilization of VHF and UHF bands which usually are not available for radar application. These bands have wavelengths comparable to the targets' size. These frequencies give to the forward scatter a larger angular width, which enables stealthy aircraft tracking.
- A passive radar is not easy to trace, since it is not emitting radio waves but only exploits existing sources of illumination.
- FM broadcasting antennas are in high altitude, with broad coverage, suitable for detecting targets.
- No need for expensive transmitters, which would also demand licensing.
- Low-cost setup, especially with the use of cheap Software-defined radios, also used in this project.

On the other hand, a PR has some disadvantages over an active radar:

- The performance of the radar is poor when the target is close to the line segment that connects the FM station and the PR's position, which is called baseline. This is due to the increased Direct Signal Interference (DSI) received from the observation antenna.

- The radio waves used are not optimized for radar use.
- Given that the signal is constantly emitted from the FM station, care must be taken in order to suppress the DSI from the observation antenna. This increases the complexity of the system.

As an illuminator of opportunity, the FM radio station of Malaxa is used. It is located approximately 7km south-east compared to the receiver located at ECE, Technical University of Crete. A 3D map with landmarks in the position of the PR setup and the FM Station is included in Fig. 1.1.

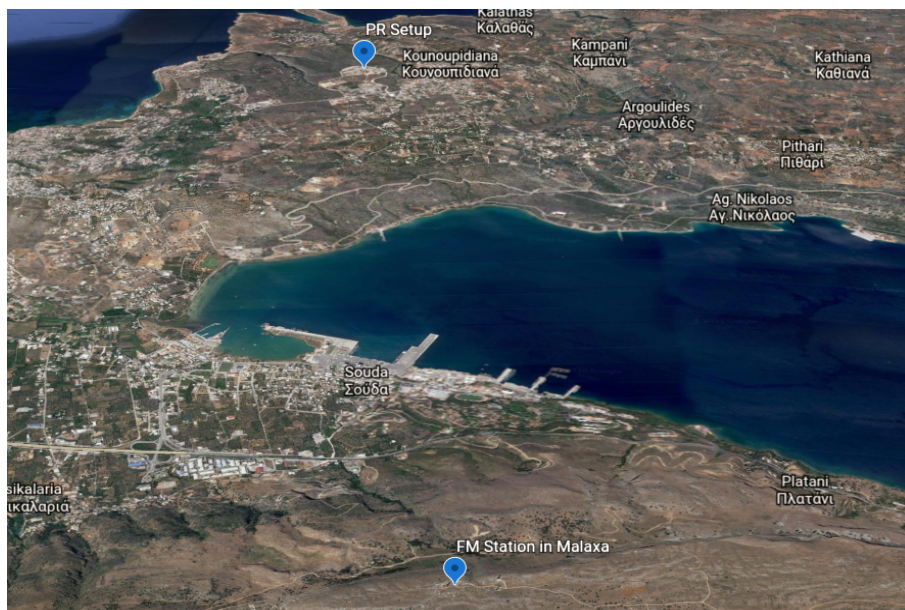


Figure 1.1: The FM station in Malaxa and the PR setup.

FM stations have the following benefits as an illumination source:

- The FM channels are accessible almost everywhere.
- They transmit signals with high power.
- There are many FM channels with different content, bandwidth and carrier frequency to choose.

The PR has various applications for military, geophysical and astronomical radio remote sensing [1]. The first operational PR was the Klein Heidelberg [2], which was used by the Germans in World War II as an early warning system for the German Air Defence. It used as an illumination source the British Chain Home radars and

---

was not detected by the Allies until October 1944. It was used late in the war, so, fortunately, it was not a defining factor for the outcome of the war. Other examples of more recent operational military PRs, according to [3], are:

- The Silent Sentry launched by Lockheed Martin the late 90s early 2000s, which uses FM radio signals to operate. It detects aircraft and airborne missiles.
- The Homeland Alerter from the Thales Company in France.
- The multiband system FM/DAB/DVT system from the Airbus Systems Defence and Space.

So it is clear that passive radars are a research field which has seen great progression over the last few years. The advance in technology of the last few decades, has allowed PRs to evolve even further.

Aside from the military purposes, it can be also used for other interesting applications such as geophysical and astronomical remote radio sensing [4]. An example is the Manastash Ridge Radar which is using FM radio signals to study ionospheric turbulence as well as meteor trails [5].

In Chap. 2, the model that describes the passive radar, along with an overview of the software and the hardware used, are presented. In Chap. 3, the mathematical model of the passive radar and the process of clutter removal, through various adaptive filtering algorithms, is described. In Chap. 4, an efficient computation method of the ARD surface is included. Chap. 5 contains experimental results produced from real-data that lead us to some conclusions, which are presented in Chap. 6.

# Chapter 2

## System overview

The electromagnetic waves emitted from the FM radio station are following different paths before they are captured by the PR antennas. The greatest part of the signal is following the direct path from the FM station to the PR receivers or it reflects from various obstacles out of interest (buildings, mountains, sea etc.) and ends up to the PR's antennas. Finally, a small portion of the emitted FM signal scatters to targets of interest and returns to the PR setup. This is depicted in Fig. 2.1.

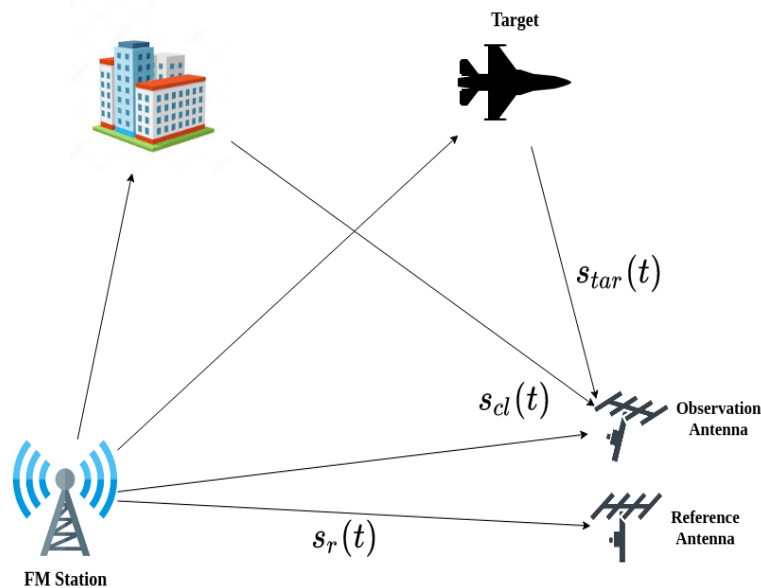


Figure 2.1: Representation of the FM signals captured by a passive radar

The target echo can be detected by pointing two antennas, one as a reference directly to the FM station and another directional antenna (observation) towards the surveillance area. The reference antenna's purpose is to receive a high SNR version of the transmitted signal. This signal will be used to suppress the clutter term and keep only the  $s_{tar}(t)$

The reference antenna receives the FM Station's signal  $s_r(t)$ , along with multipath and clutter. Due to line of sight reception, the SNR is high and therefore, the clutter of the reference antenna can be neglected. This simplification is for computational

efficiency and reduced complexity of the system, while also, to avoid degrading the SNR of the reception. As a result, the reference signal is denoted as  $s_r(t)$ .

A PR setup has the characteristic that the emission from the radio station has a duty cycle of 100%. This means that at any given time the observation antenna is receiving both the direct signal, which is called direct signal leakage and the reflections from static objects. This unwanted part of the observation is called Direct Signal Interference (DSI) or clutter and it is symbolised in Fig. 2.1 as  $s_{cl}(t)$ .

When a target appears in the surveillance area, the reflection signal that the observation antenna receives is denoted as  $s_{tar}(t)$  and is hidden inside the DSI. The DSI is mostly on the zero Doppler and zero range bin. The value of this bin causes its sidelobes on both range and Doppler to be several orders of magnitude higher than the target echoes [6]. Therefore, it needs to be suppressed by both angular nulling and the application of an adaptive filter to the observation antenna's signal. This is done by using the reference antenna's input,  $s_r(t)$ , because the DSI is consisting from scaled and delayed replicas of the reference signal [7]. Then, the drop of the overall noise floor below that of the target's reflections, will allow the PR to detect the weak target echoes. Therefore, the observation signal, which is received by the observation antenna, is the sum of the target echo, the clutter term and additive noise.

## 2.1 Software Overview

The reception of the signals is performed using GNURadio. Then, the samples are passed into Matlab for the processing phase, which is depicted in Fig. 2.2.

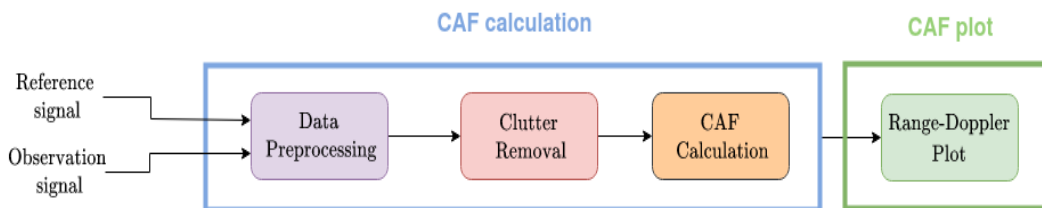


Figure 2.2: Stages of the PR processing.

First, two data blocks of constant size are inserted from the reference and the observation antenna.

In the Data preprocessing block the data are:

1. shifted to the central frequency of the FM Station of interest,
2. decimated to fit the bandwidth of the station used,

3. aligned, by finding the peak of the cross-correlation of the reference and the observation signal. This is done, in order to alleviate any constant offset that may be inserted between the two datasets.

Then, the clutter removal operation is reducing the noise floor to extract the target echoes  $s_{tar}(t)$ . This is done by various algorithms as explained in Chap. 3.

Assuming that we have extracted the targets' signals  $s_{tar}(t)$  the Cross-Ambiguity function (CAF) is calculated. This 2D matrix consists of a number of Amplitude-Range-Doppler (ARD) frames, depicting the target's Doppler on one axis and its range on the other. The amplitude is depicting the strength of the target's echo. The Doppler contains the information of the target's speed. The process of calculating the CAF is described in Chap. 4 in detail.

In addition, after the ARD surfaces are calculated, a Cell-Averaging Constant False Alarm Rate (CA-CFAR) is used to extract the targets from background noise and remaining clutter. This method is analysed in Chap. 4.

## 2.2 Hardware

### 2.2.1 Antennas

#### Reference Antenna

In order to achieve the highest possible SNR and gather accurate replicas of the transmitted signal, line of sight (LOS) with the FM Station should be established. The antenna is a vertically polarised monopole, shown in Fig. 2.3.



Figure 2.3: The reference antenna and the FM Station on the opposing mountain in the area of Malaxa.

### Observation Antenna

It is a Small Five-Element Yagi for 87.5-108 MHz, designed by K6STI [8], with 5.2 to 7.2 dBd forward gain and maintaining that all backlobes are below the forward gain by at least 20db. This helped restricting the effects of the DSI and the multipath. The antenna is shown in Fig. 2.4.

For the construction for the antenna, aluminium rods of 10mm were used. The boom is a plastic tube with 50mm diameter. In order to attach the rods to the boom, resin support block clamps were used. Those clamps have a metal base, which was extended by welding two small ring shaped metal pieces to their metal base. In this way, the clamps were installed with the use of rivets, one on each extension. Bearing in mind that the DSI must be eliminated as much as possible, observation antenna is placed at an angle that puts the direct FM station's signal at a null in the radiation pattern. Also, shielding the observation antenna is going to help reducing the amount of the DSI. In our case, it is located in a wall surrounded area with clear view of the sky, as depicted in Fig. 2.4. Also, the polarization of the antenna is vertical.



Figure 2.4: The observation antenna.

In Fig. 2.4, the walls and obstacles are between the antenna and the FM station, reducing the effect of the direct FM station's signal leakage.

### 2.2.2 SDR

Two different low-cost Software-Defined Radios (SDR) setups were used.

#### RTL-SDR

The first consists of two RTL2832U SDRs costing around 8\$ each.

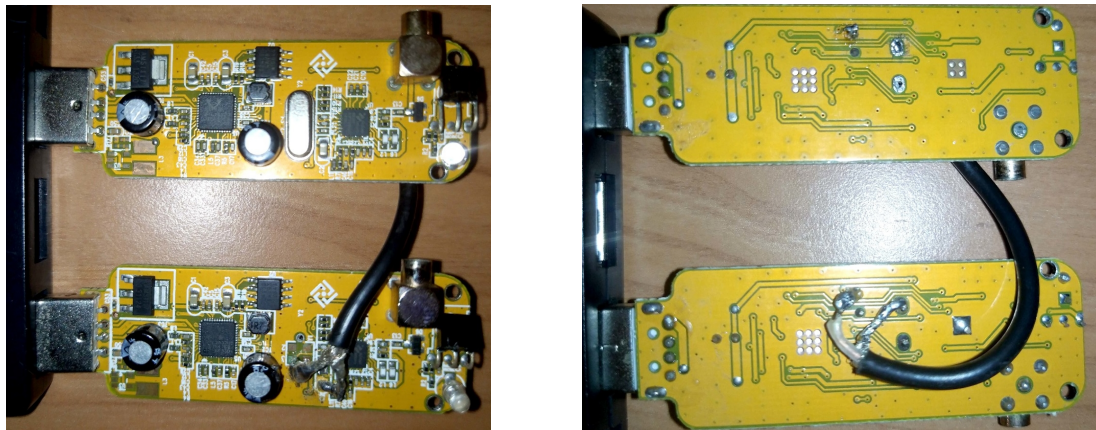


Figure 2.5: The two RTL-SDRs with the connected clock.

Because the samples of the two RTLs must be aligned or in other words, sampled with the exact same frequency, they were connected to a common clock source. Furthermore, during the Preprocessing stage of Fig. 2.2 described in Sec. 2.1, a cross-correlation was done between the two sets of samples, one from the reference and one from the observation signal, which were captured simultaneously. With this process a varying time offset between the two signals was corrected. This was probably due to an inconsistency in the sampling interval, despite the common clock source. This offset is varying between each chunk of data and must be calculated for each one separately. Also, their ADC, has a dynamic range of 8 bits, only.

#### LimeSDR USB

A LimeSDR-USB is shown in Fig. 2.6. It costs around 300\$. It consists of 2 receivers and has an ADC of 12 bits, which improves the performance of the PR.

The ADC resolution of the LimeSDR USB is higher in comparison to the RTL-SDR (12 bits vs 8 bits) which is important. It allows better tracking of the weak echoes, enabling more accurate suppression of the DSI, due to the reference signal's better correlation with the DSI.



Figure 2.6: A LimeSDR-USB used for receiving the Reference and Observation signals.

Also, it inserts minimal to no time offset between the reference and the observation signals, in contradiction to the RTL-SDR setup. Therefore, the measurements are more reliable.

# Chapter 3

## Clutter removal

Clutter or Direct Signal Interference (DSI) is caused by leakage of the direct FM station signal to the observation antenna, as well as signal reflected from targets that are of no interest. Examples are natural objects, such as the ground, mountains, sea, birds and static objects like buildings. Clutter could be thousands of times stronger than the target's reflections. Therefore, its removal is necessary.

### 3.1 Continuous-time model

To derive the clutter algorithms, some assumptions are needed. The baseband reference signal  $s_r(t)$  is the signal received by the reference antenna, which is pointing towards the FM station and is described as follows:

$$s_r(t) = A_r s_{tx}(t - \frac{R_{SR}}{c}) + v_r(t), \quad (3.1)$$

where  $s_{tx}(t)$  is the FM station's transmitted signal,  $A_r$  is a complex amplitude number representing the channel's effect in the propagation of the signal,  $R_{SR}$  is the distance (kms) between the station and the receiver,  $c$  is the speed of light ( $\frac{kms}{sec}$ ) and  $v_r(t)$  is the complex white Gaussian noise added. Because the receiver is not moving, the delay  $\tau_{SR} = \frac{R_{SR}}{c}$  is constant.

In this implementation, the effect of the multipath and clutter to the reference signal was ignored. This simplification was possible due to the high SNR of the FM signal that the reference antenna receives. To maintain the high SNR value, line of sight connection between the reference antenna and the FM station should be established. Removing the clutter from the reference signal would not cause any significant improvement and it would mostly increase the complexity of the system, along with the computational cost of the implementation. The consequences are the appearance of false peaks closer to the receiver at the Range-Doppler surface. This is due to the constant delay  $\tau_{SR}$  increasing, if the path of the transmitted signal is longer than the straight baseline one, due to multipath.

Then, the delay between the reference signal and the targets' reflections would be

reduced, along with the range measurement of the targets. Although it may seem a good idea to filter out the clutter from the reference antenna, it would increase significantly the computational cost and the complexity of the system. Also, it would risk decreasing the SNR of  $s_r(t)$ , which is an important factor for the PR's operation. An easy way to reduce the multipath of the reference signal would be to use a directional antenna to capture it.

Also,  $s_o(t)$  is the total signal received by the observation antenna. The equation which describes the observation signal is the following:

$$s_o(t) = s_{tar}(t) + s_{cl}(t) + v_o(t). \quad (3.2)$$

where  $s_{cl}(t)$  is the clutter part of the signal,  $s_{tar}(t)$  are the targets' reflections which are hidden inside the clutter and  $v_o(t)$  is the additive complex white Gaussian noise. The observation antenna must be of high gain, in order to detect the weak target echoes. Therefore, the highly directive 5 element FM Yagi antenna of Chap. 2 was used. In comparison with the reference signal, the faded reflected echoes are now amidst strong clutter signals. Thus, a method for clutter removal is essential to extract those target reflections.

The difference between  $s_{cl}(t)$  and  $s_{tar}(t)$  is that clutter is a linear combination of scaled and delayed replicas of the reference signal, while  $s_{tar}(t)$  is shifted by the targets' Doppler frequency. Clutter may also consist of signal reflections from objects that move e.g. passing vehicles or trees moving from the wind. The speed and therefore the Doppler shift of these objects is small compared to the actual targets [9]. The above can be described in the following equation:

$$s_o(t) = \underbrace{\sum_{k=0}^{M-1} w_k s_{tx}\left(t - \frac{R_{cl,k}}{c}\right) \exp(j2\pi f_{cl,k}t)}_{\text{Direct signal leakage and clutter}} + \underbrace{\sum_{k=0}^{N-1} b_k s_{tx}\left(t - \frac{R_{e,k}}{c}\right) \exp(j2\pi f_{e,k}t)}_{\text{Target reflections}} + v_o(t) \quad (3.3)$$

where out of the three terms above, the first one represents the direct signal leakage and the clutter, the second the targets' echoes and the third the additive complex Gaussian noise. The  $w_k$  and  $b_k$  terms represent the complex amplitude and the phase induced by the channels' effect. In the case of  $\{b_k\}$  the targets' RCS (Radar cross-section) also plays a role in the value. The  $w_k$  term for  $k = 0$  represents the direct signal leakage, while for  $k = 1, \dots, M - 1$  represents the clutter returns.

$R_{cl,k}$  with  $k = 0, \dots, M - 1$  is the distance of the various paths that the transmitted

FM signal has followed until it reached the observation antenna except from the target returns. For  $k = 0$ ,  $R_{cl,0}$  will be the direct path from the FM Station to the observation antenna (baseline), which is considered the same with  $R_{SR}$  due to being relatively close, in comparison to the distance from the FM Station.  $R_{e,k}$  is the distance that the target's echo has covered from the FM station to the observation antenna.

In the clutter,  $M$  represents significant clutter reflections that the observation antenna has received, while  $N$  is the number of targets that the radar has detected. A constant Doppler term was added to the clutter term to model those objects that move slightly. In the targets' echoes, a Doppler term is added to identify the target's speed, which typically has a greater value than this of the clutter's objects ( $f_{e,k} > f_{cl,m}$ ).

## 3.2 Discrete-time model

For the following methods, digital signal processing is needed. The samples are taken every  $T_s$  seconds, such that  $t = nT_s$ . Therefore, the discrete signals are a function of discrete time  $nT_s$ , which is represented by square brackets. The signals'  $s_r[n]$  and  $s_o[n]$  I/Q baseband samples are captured with the help of GNURadio Companion. Then, they are given as input to the software in Matlab.

The discrete equivalent of Eq. 3.3 can be described as follows:

$$s_o[n] = \underbrace{\sum_{k=0}^{M-1} w_k s_r[n - d_{cl,k}]}_{\text{DSI}} + \underbrace{\sum_{k=0}^{N-1} b_k s_r[n - d_{e,r}] \exp\left(\frac{j2\pi f_{e,k} n}{F_s}\right)}_{\text{target reflections}} + v_o[n] \quad (3.4)$$

where  $v_o[n]$  is complex Gaussian white noise and  $d_{cl,k}$  is the delay in samples of each of the  $M$  DSI reflections. Also,  $s_r[n]$  is the discrete reference signal which has substituted the  $s_{tx}[n]$ . This simplification can occur since the delay between the reference antenna and the FM station is constant and can be removed, while also there is a high SNR reception of the  $s_r[n]$  from the reference antenna due to LOS. The small constant Doppler term of the DSI of Eq. (3.3) due to slight movements is neglected. This was done to simplify the explanation of the adaptive filtering algorithms of Sec. 3.3 and because most of the clutter reflections are from static objects.

The target reflections are comprised of  $N$  echoes, which denotes the number of the significant target reflections, the  $\{b_k\}$  term which denotes the channel's effect and  $d_{e,r}$  the corresponding delay of the target in samples. Also, an exponential term is added to model the frequency shift  $f_{e,k}$  due to the Doppler effect. The  $F_s$  term is the

sampling rate.

The target reflections of (3.4), denoted as  $s_{tar}[n]$  could be also given as follows:

$$s_{tar}[n] = s_o[n] - \sum_{k=0}^{M-1} w_k s_r[n - d_{cl,k}], \quad (3.5)$$

where the unknown terms are the number of reflection  $M$ , the complex channel effect  $\{w_k\}$ , the delay  $d_{cl,k}$  and the complex Gaussian noise  $v_o[n]$ .

The difference between  $s_{cl}[n]$  and  $s_{tar}[n]$  of Eq. (3.4) is the Doppler term, which is used in order to extract the speed of the targets. A useful property that is going to be used in order to solve the clutter removing problem is that complex exponential functions of different frequencies are orthogonal to one another under some constraints, which will be proven below:

If  $f_k \neq f_p$ , then:

$$\begin{aligned} \langle e^{j2\pi f_k t}, e^{j2\pi f_p t} \rangle &= \int_0^T e^{j2\pi f_k t} \overline{e^{j2\pi f_p t}} dt = \int_0^T e^{j2\pi(f_k - f_p)t} dt \\ &= \frac{1}{j2\pi(f_k - f_p)} [e^{j2\pi(f_k - f_p)t}]_0^T \\ &= \frac{1}{j2\pi(f_k - f_p)} [e^{j2\pi(f_k - f_p)T} - e^0] \\ &= 0 \quad \text{if } |f_k - f_p| = \frac{k}{T}, \quad \text{with } k \in \mathbb{N}^*. \end{aligned} \quad (3.6)$$

If  $f_k = f_p$ , then:

$$\langle e^{j2\pi f_k t}, e^{j2\pi f_k t} \rangle = \int_0^T e^{j2\pi f_k t} \overline{e^{j2\pi f_k t}} dt = \int_0^T e^{j2\pi(f_k - f_k)t} dt = \int_0^T 1 dt = T \quad (3.7)$$

Therefore, complex exponentials with different frequencies are orthogonal, when the frequencies differ by multiples of  $1/T$ , with  $T$  denoting the Coherent Processing Interval (CPI). The CPI is, in other words, the size of each chunk of data that we process. This partition occurs to produce multiple Range-Doppler frames and reduce the processing load.

The relation between the CPI length and the Doppler resolution is the inverse one. The Doppler resolution is the minimum difference between Doppler frequencies that can be distinguished.

As a result, if the targets' reflected signal has a frequency shift and the summation is over a sufficiently long time interval, the reference signal and targets' echoes will be

orthogonal. Therefore, removing a component of the signal will not affect the other components of the signal with frequency difference  $\frac{k}{T}$ , with  $k \in \mathbb{Z}$ .

The DSI as shown in Eq. 3.5 is comprised of scaled and delayed replicas of the reference signal. Hence, eliminating those replicas successfully, will drop the level of the sidelobes of the cross-correlation of the reference signal and the clutter reflections. As a result, the target echoes which are hidden inside the clutter will be revealed.

The scaling factors  $w_k$  of Eq. (3.5) and the delay of each clutter reflection are unknown and therefore, adaptive filtering is used to compute them.

### 3.3 Adaptive filters

As described in [10], [9], adaptive filtering can be used for interference cancellation on passive radar applications. This application is described in Fig. 3.1 .

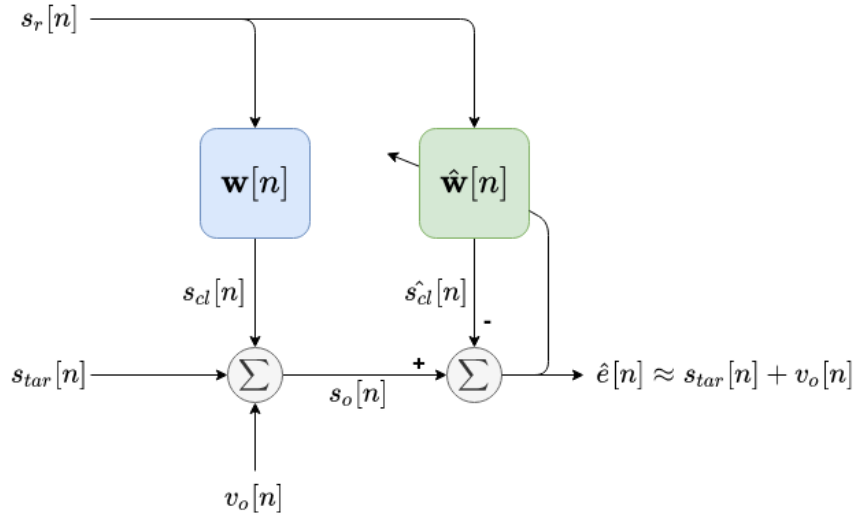


Figure 3.1: The adaptive filter's generalized structure for interference cancellation.

The observation signal contains the target echoes along with clutter and noise. As mentioned previously, clutter is comprised from scaled and delayed replicas of the reference signal. The problem is that neither the scale nor the delay of the clutter reflections are known a priori. Therefore, the purpose of the Adaptive Filter is to estimate the clutter term,  $\hat{s}_{cl}[n]$  in Fig. (3.1) and subtract it from the observation signal. As a result, this process will reduce the noise floor and the targets will appear. The noise floor is increased due to the large value of the zero-Doppler and zero-range bin. This large value is caused due to direct signal and multipath and is causing increased sidelobes and the target echoes are hidden below this level.

As it was proven in Eq. (3.6), exponentials with frequencies that differ by  $\frac{k}{T}$ , where  $T$  is the CPI and  $k \in \mathbb{Z}$ , are orthogonal. This principle is used in Fig. 3.1. The observation signal is the summation of the target signals, DSI and noise. The DSI can be subtracted only when the orthogonality of Eq. (3.6) is satisfied.

### 3.3.1 Least-Squares

In Least-Squares [10], [7], the data are divided into blocks of constant size and the  $w_k$  terms of Eq. (3.4) are computed in each block separately. The size of these blocks is set equal to the Coherent Processing Interval.

For the LS filter,  $\mathbf{y}$  is the observation signal while  $\mathbf{x}_k$  is the reference signal delayed by  $k$  samples. Both vectors contain  $L$  consecutive samples each.  $\mathbf{X}$  is a matrix whose columns contain  $\mathbf{x}_k$  with  $k = 0, \dots, M - 1$ , where  $M$  is the number of the clutter reflections. Therefore,  $\mathbf{X}$  has dimensions  $L \times M$  with the assumption that  $L > M$ , which will be analysed later in this Section. Also,  $\mathbf{w}$  is a vector of length  $M$ , that denotes the  $w_k$  scalars of Eq. (3.4).

LS filtering can be described as follows:

$$\boldsymbol{\epsilon} = \mathbf{y} - \mathbf{X}\mathbf{w}. \quad (3.8)$$

Eq. (3.8) is described in the following matrix-vector representation:

$$\begin{bmatrix} \epsilon[0] \\ \epsilon[1] \\ \vdots \\ \epsilon[L-1] \end{bmatrix} = \begin{bmatrix} y[0] \\ y[1] \\ \vdots \\ y[L-1] \end{bmatrix} - \begin{bmatrix} s_r[0] & 0 & \cdots & 0 \\ s_r[1] & s_r[0] & \cdots & 0 \\ \vdots & \vdots & \ddots & \vdots \\ s_r[M-1] & s_r[M-2] & \cdots & s_r[0] \\ \vdots & \vdots & & \vdots \\ s_r[L-1] & s_r[L-2] & \cdots & s_r[L-M] \end{bmatrix} \begin{bmatrix} w_0 \\ w_1 \\ \vdots \\ w_{M-1} \end{bmatrix} \quad (3.9)$$

In Eq. (3.9),  $\boldsymbol{\epsilon}$  and  $\mathbf{y}$  are vectors of length  $L$ .  $\mathbf{X}$  is a matrix comprised of  $M$  columns, each containing  $L$  consecutive samples from the reference signal  $\mathbf{s}_r$ , which are delayed by one sample along the columns of the matrix. It is modelling the possible delays of each clutter path. The samples before  $s_r[0]$  are considered zero.  $\mathbf{w}$  is a vector of length  $M$  containing the  $w_k$  complex numbers of Eq. (3.4), which model the complex amplitude channel term of each clutter reflection.

In Eq. (3.8),  $\mathbf{X}\mathbf{w}$  is trying to model the clutter signal. Subtracting a sufficient estimate of the clutter from the observation signal leaves us with the target echo

vector  $\mathbf{s}_{tar}$  along with additive complex Gaussian noise:

$$\boldsymbol{\epsilon} = \mathbf{s}_{tar} + \mathbf{v}_o. \quad (3.10)$$

The goal of this process is to minimize  $\epsilon$  or in other words subtract as much as possible of the clutter from the observation antenna. Therefore, we search for the quantity of:

$$\arg \min_{\hat{\mathbf{w}}} \|\mathbf{y} - \mathbf{X}\hat{\mathbf{w}}\|_2^2. \quad (3.11)$$

Eq. (3.11) can be reduced to an ordinary least-squares problem whose solution is the following:

$$\hat{\mathbf{w}} = \mathbf{X}^\dagger \mathbf{y} \Leftrightarrow \hat{\mathbf{w}} = (\mathbf{X}^H \mathbf{X})^{-1} \mathbf{X}^H \mathbf{y}. \quad (3.12)$$

The LS algorithm's linear transversal filter model is shown in Fig. 3.2.

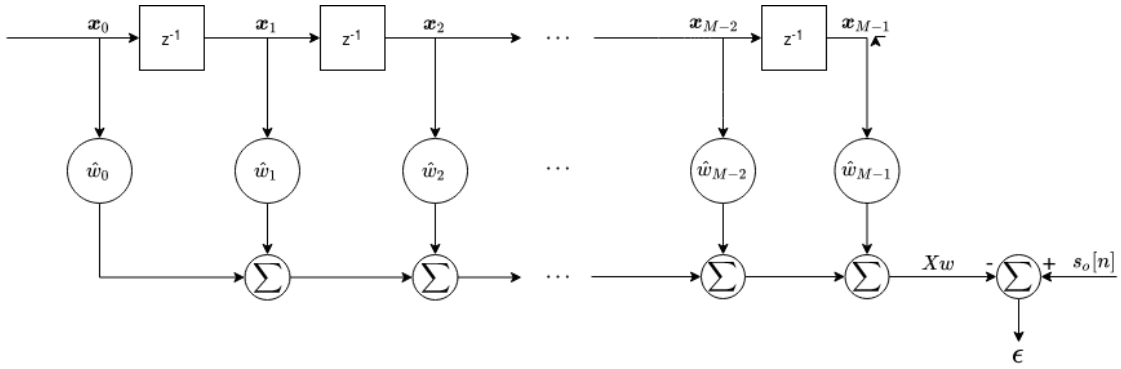


Figure 3.2: Model of the linear transversal filter with the  $\hat{\mathbf{w}}$ .

In fact,  $(\mathbf{X}^H \mathbf{X})$  could be ill-conditioned (nearly singular) and cause  $\hat{\mathbf{w}}$  to have more than one solution.

The rank of an  $M \times N$  matrix is a non-negative integer and it cannot be greater than either  $M$  or  $N$ . That is,

$$\text{rank}(\mathbf{A}) \leq \min(M, N). \quad (3.13)$$

When the equality is satisfied the matrix  $\mathbf{A}$  is full-rank. Because  $\mathbf{X}$  is a matrix of dimensions  $L \times M$  and  $\mathbf{X}^H$  of  $M \times L$ , their product  $\mathbf{X}^H \mathbf{X}$  has dimensions  $M \times M$ .

Also,

$$\text{rank}(\mathbf{X}^H \mathbf{X}) \leq \min(\text{rank}(\mathbf{X}^H), \text{rank}(\mathbf{X})) \leq \min(\min(M, L), \min(L, M)). \quad (3.14)$$

In addition, the rank relation between a complex matrix  $\mathbf{A}$  and its Hermitian  $\mathbf{A}^H$ , is shown below:

$$\text{rank}(\mathbf{A}) = \text{rank}(\mathbf{A}^H). \quad (3.15)$$

From Eq. (3.14) and (3.15) the rank of  $\mathbf{X}^H \mathbf{X}$  is given by:

$$\text{rank}(\mathbf{X}^H \mathbf{X}) \leq \min(M, L). \quad (3.16)$$

In order for  $\mathbf{X}^H \mathbf{X}$  to be full-rank with rank  $M$ , the following conditions must be satisfied:

- $L \geq M$  or, in other words, larger CPI length than filter length.
- The equality of (3.16)

In order to avoid any linear dependencies inside the matrix  $\mathbf{X}^H \mathbf{X}$  that reduces the rank below  $M$ , a simple L2-norm Tikhonov regularization technique is used and Eq. (3.12) becomes:

$$\hat{\mathbf{w}} = (\mathbf{X}^H \mathbf{X} + \mathbf{\Gamma}^H \mathbf{\Gamma})^{-1} \mathbf{X}^H \mathbf{y}, \quad (3.17)$$

where  $\mathbf{\Gamma} = \alpha \mathbf{I}$ , with  $\mathbf{I}$  an  $M \times M$  identity matrix. After the calculation of  $\hat{\mathbf{w}}$ , the targets' echoes are computed as follows:

$$\hat{\mathbf{e}} = \mathbf{y} - \mathbf{X} \hat{\mathbf{w}} \Leftrightarrow \mathbf{s}_{tar} + \mathbf{v}_o = \mathbf{y} - \mathbf{X} \hat{\mathbf{w}}. \quad (3.18)$$

As long as the noise level  $\mathbf{v}_o$  is low compared to  $\mathbf{s}_{tar}$ , the algorithm will converge and it will appear in the Range-Doppler surface of the radar.

### 3.3.2 Least-Mean-Square

The Least-Mean-Square (LMS) filter (Widrow and Hoff, 1960) [11] is a stochastic gradient-based or iterative algorithm [10], [12], [13]. This means that it is updating the filter coefficients for the entire length of the data, in contradiction with block type algorithms, such as the LS filter, that separate the data into blocks of constant size to process each of them independently. It is a computationally efficient algorithm

since it does not contain any matrix inversions, unlike LS. The LMS algorithm was not used for this PR due to its need for parameter fine tuning. Nevertheless, since it is the basis of the next iterative type algorithms used for the PR, its derivation is included.

The algorithm is based on a filter coefficient vector  $\mathbf{w} \in \mathbb{C}^{M \times 1}$ , which is updated with each sample of the input signals,  $s_r[n]$  and  $s_o[n]$ . The vector  $\mathbf{w}$  is updated as in Eq. (3.19):

$$\mathbf{w}[n+1] = \mathbf{w}[n] + \mu \mathbf{u}[n] e^*[n], \quad (3.19)$$

where  $\mathbf{u}[n]$  is the input vector, denoted as follows:

$$\mathbf{u}[n] = \begin{bmatrix} s_r[n - (M - 1)] & s_r[n - (M - 2)] & \dots & s_r[n] \end{bmatrix}^T. \quad (3.20)$$

The error scalar  $e[n]$ , which is also the clutter removed signal, is calculated as follows:

$$e[n] = s_o[n] - y[n], \quad (3.21)$$

where  $y[n]$  is the output of the algorithm, which is computed as follows:

$$y[n] = \mathbf{w}^H[n] \mathbf{u}[n], \quad (3.22)$$

The parameter  $\mu$  of Eq. 3.19 is a positive constant step size parameter. This parameter must satisfy the following:

$$0 < \mu < \frac{2}{\lambda_{max}}, \quad (3.23)$$

where  $\lambda_{max}$  denotes the largest eigenvalue of the autocorrelation matrix  $\mathbf{R}$  of the reference vector  $\mathbf{u}[n]$ . According to [12], if  $\lambda_{max}$  is difficult to compute then the inequality can change accordingly:

$$0 < \mu < \frac{2}{\text{tr}(\mathbf{R})}, \quad (3.24)$$

The term  $\text{tr}(\mathbf{R})$  in Eq. (3.24) is easier to compute than  $\lambda_{max}$  and the purpose of using it is explained as follows:

$$\text{tr}(\mathbf{R}) = \sum_{k=0}^{M-1} \lambda_k \geq \lambda_{max} \Rightarrow \frac{2}{\text{tr}(\mathbf{R})} \leq \frac{2}{\lambda_{max}}. \quad (3.25)$$

In this way, a stricter but easier to compute constraint is imposed to the value of  $\mu$ .

The transversal filter of the LMS algorithm is presented in Fig. 3.3. The LMS

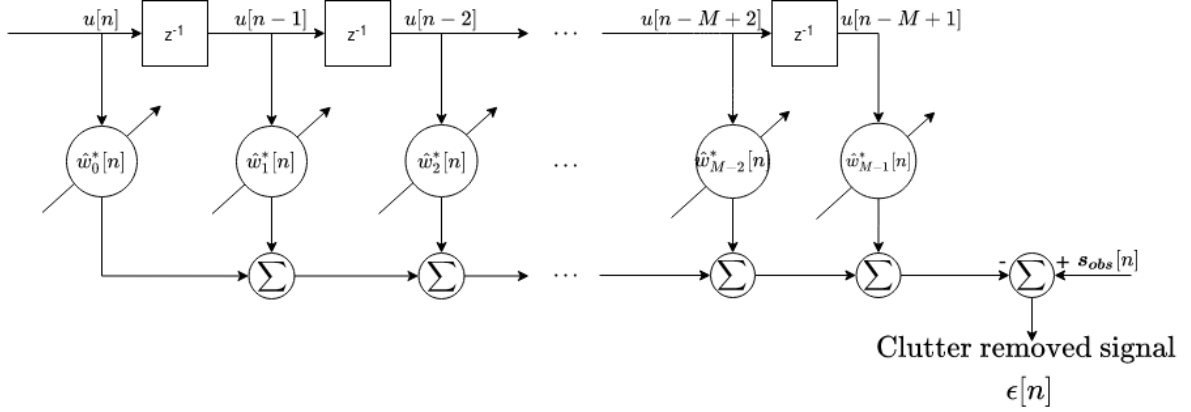


Figure 3.3: The transversal filter of the LMS algorithm.

filter's estimation is a linear combination of the reference signal. As a result, when the orthogonality principle of Eq. 3.6 is satisfied, the LMS will only affect the DSI's value. The NLMS, BNLMS and FBNLMS, which will be presented in the next sections are based on the same principle.

If the value of  $\mu$  is small, then the algorithm will converge at a slower rate and its reaction to changes will be less rapid, failing to suppress the clutter. In the opposite case, where  $\mu$ 's value is higher, the algorithm will have quicker reactions but with an increased risk of misjudgement. Therefore, optimizing the  $\mu$  value is essential for good operation of the algorithm [10], [12].

Finding the optimal value for  $\mu$  is a difficult task, since it depends on both the length of the filter and the power of the reference signal. This power is changing when the reference SNR is changing. This could be due to the use of a different FM channel or FM broadcasting station or by changing the position of the antennas. Therefore, hand tuning it each time held us back from using this algorithm for the PR's operation.

Also, when the parameter  $\mathbf{u}[n]$  has a large value, although the algorithm has converged, it causes significant misjudgement errors. This problem is called gradient noise amplification [10]. The next algorithms (NLMS, BNLMS, FBNLMS) are the iterative algorithms that were used for the PR. They are the descendants of the LMS algorithm. They solve some of its problems regarding parametrization, gradient noise amplification and computational efficiency.

### 3.3.3 Normalized Least-Mean-Square

The normalized LMS (NLMS) algorithm copes with the LMS algorithm's constraint of the  $\mu$ 's value regarding the total input power of the reference signal vector  $\mathbf{u}[n]$ . This is shown in Eq. (3.24). This is done as follows:

$$\mathbf{w}[n+1] = \mathbf{w}[n] + \frac{\mu}{b + \mathbf{u}^H[n]\mathbf{u}[n]} \mathbf{u}[n]e^*[n]. \quad (3.26)$$

The number  $b$  is a small number (i.e. 0.001) used to prevent numerical instabilities while  $\mu$  is divided by the reference signal's energy in each iteration. In this way, the algorithm becomes independent from the total input power of  $\mathbf{u}[n]$ , which is suitable for the PR operation, since many factors can change the reference signals power. The constant step size parameter of the LMS algorithm will become time-varying, resulting, potentially, to a faster rate of convergence than LMS and a decreased possibility for misjudgements. The derivation of the NLMS can be produced by using Lagrange multipliers, as shown in [10], [12].

Also, it reduces the gradient noise amplification problem by normalizing the power of the input in each step.

The trade-off with the NLMS is that it is more computationally expensive than the LMS algorithm. The next algorithms (BNLMS, FBNLMS) will be used to reduce the computational cost of the NLMS and LMS algorithms, while also improve their convergence rate and reduce their misjudgement errors.

### 3.3.4 Block Normalised Least-Mean-Square

The block NLMS (BNLMS) [14] algorithm is an extension of the NLMS algorithm, where instead of updating the weight vector  $\mathbf{w}$  in each iteration, it is updated once in each block of data. The length  $\hat{L} > 1$  of each block is determined by the user. Therefore, if the input vector has length  $L$ ,  $\mathbf{w}$  will be updated  $\lfloor L/\hat{L} \rfloor$  times instead of  $L$ . It is obvious that the BNLMS has a higher computational efficiency due to the reduction of the weight updates. The discrete time  $n$  becomes  $n = k\hat{L} + p$ , where  $p = 0, 1, \dots, \hat{L} - 1$  and  $k = 0, 1, \dots, \lfloor \frac{N}{\hat{L}} \rfloor - 1$ . The formula, which is describing the coefficient updates, is the following:

$$\mathbf{w}[k] = \mathbf{w}[k-1] + \mu_B \sum_{p=0}^{\hat{L}-1} e[k\hat{L} + p] \mathbf{u}[k\hat{L} + p], \quad (3.27)$$

where the term  $\mathbf{e}[n]$  denotes the error vector, which contains the last  $L$  calculations of the scalar  $e$ , as described in the previous algorithms. The term  $\mu^B$  will be described as follows:

$$\mu^B = \frac{\mu}{\hat{L}(b + \mathbf{u}^H[n]\mathbf{u}[n])}. \quad (3.28)$$

The reason that the term  $\mu^B$  is divided by  $\hat{L}$ , is that the term  $\sum_{p=0}^{\hat{L}-1} \mathbf{e}[k\hat{L} + p]\mathbf{u}[k\hat{L} + p]$  is actually computing corrections for  $\hat{L}$  samples and then at the end of the block they are all summed up. As a result, when those corrections are divided by  $\hat{L}$  an unbiased time average is computed.

For the PR operation, the length of the reference vector  $\mathbf{u}$  and the length of the filter  $M$  were chosen the same.

### 3.3.5 Fast Block Normalised Least-Mean-Square

The fast BNLMS (FBNLMS) is the most computationally efficient algorithm that was examined in this thesis. It was originally proposed by Ferrara(1980) [15] and in 2013, it was examined for the operation of clutter removing in PR [14].

The LMS, NLMS, BNLMS are all algorithms of the time-domain. BNLMS can be computed efficiently in the frequency-domain, where the efficiency of this algorithm relies on. More specifically, according to [10], the operations of the time-domain BNLMS that limit its efficiency and could be improved by exploiting the frequency-domain are the following:

- The equation  $y[n] = \mathbf{w}^H[k]\mathbf{u}[n]$  of (3.22), which is a linear convolution.
- The gradient vector  $\sum_{p=0}^{\hat{L}-1} \mathbf{e}[k\hat{L} + p]\mathbf{u}[k\hat{L} + p]$ , which is used to update the filter coefficients  $\mathbf{w}$ . It is a linear correlation between the tap inputs of the filter and the error.

The Fast Fourier Transform (FFT) can calculate the above operations in the frequency-domain very efficiently, rather than calculating them in time, as in BNLMS.

Furthermore, the length of the blocks is chosen to be the same with the size of the vector  $\mathbf{u}$  to have the maximum speedup. For this length a power of 2 is chosen, because then FFT will be computed efficiently.

There are two methods to speed up the calculation of the fast convolution, which is the calculation of the linear convolution using the DFT. These are the overlap-

save and overlap-add methods. For this algorithm, the overlap-save method with 50 percent overlap is implemented.

First of all, the length of each block is equal to  $L$ . The filter length  $M$  will be set equal to  $L$ . Therefore, the FFT length  $N$  will be  $N = 2M$ , due to the overlap-save method. The filter coefficients will be calculated as follows:

$$\hat{\mathbf{W}}[k] = \text{FFT}_N \begin{bmatrix} \hat{\mathbf{w}}[k] \\ \mathbf{0}_{M \times 1} \end{bmatrix}, \quad (3.29)$$

where  $\text{FFT}_N$  denotes the  $N$ -point Fast Fourier Transform and  $\hat{\mathbf{w}}[k]$  the filter coefficients in time.

Then, the input vector  $\mathbf{U}$  with dimensions  $N$ -by-1 is formed as follows:

$$\mathbf{U}[k] = \text{FFT} \left[ \underbrace{u[kM - M], \dots, u[kM - 1]}_{(k-1) \text{ block}}, \underbrace{u[kM], \dots, u[kM + M - 1]}_{k \text{ block}} \right]^T. \quad (3.30)$$

Then, by applying the overlap-save method in Eq. (3.22), the output  $\mathbf{y}[k]$  is formed as follows:

$$\mathbf{y}^T[k] = [y[kM], y[kM + 1], \dots, y[kM + M - 1]] = \quad (3.31)$$

$$= \text{last } M \text{ elements of } \text{IFFT}[\mathbf{U}[k] \odot \hat{\mathbf{W}}[k]], \quad (3.32)$$

with  $\odot$  denoting the Hadamard product. The first  $M$  elements are discarded, since they correspond to a circular convolution.

Next, the correlation  $\sum_{p=0}^{\hat{L}-1} \mathbf{e}[k\hat{L} + p] \mathbf{u}[k\hat{L} + p]$  will be computed. First, the  $M$ -by-1 desired response vector is the following:

$$\mathbf{d}[k] = [s_{obs}[kM], s_{obs}[kM + 1], \dots, s_{obs}[kM + M - 1]]^T, \quad (3.33)$$

and the  $M$ -by-1 error vector is:

$$\mathbf{e}[k] = [e[kM], e[kM + 1], \dots, e[kM + M - 1]]^T = \mathbf{d}[k] - \mathbf{y}[k]. \quad (3.34)$$

Then, the error vector  $\mathbf{e}$  will be transferred to the frequency-domain as follows:

$$\mathbf{E}[k] = \text{FFT} \begin{bmatrix} \mathbf{0}_{M \times 1} \\ \mathbf{e}[k] \end{bmatrix}. \quad (3.35)$$

Correlation operation can be transformed to convolution when one of the sequences has its order reversed. As a result, the overlap-save method for fast correlation is actually employed by placing the zeros before the block separated input vector  $\mathbf{e}[k]$ , in contrast to the linear convolution's case of Eq. (3.29).

Accordingly, instead of preserving only the last elements, as in the linear convolution, in the linear correlation the equation changes as follows:

$$\phi[k] = \text{first } M \text{ elements of } \text{IFFT}[\mathbf{U}^H[k] \odot \mathbf{E}[k]]. \quad (3.36)$$

Then, the coefficients of the filter are updated:

$$\hat{\mathbf{w}}[k+1] = \hat{\mathbf{w}}[k] + \mu \cdot \text{FFT} \begin{bmatrix} \phi[k] \\ \mathbf{0}_{M \times 1} \end{bmatrix}. \quad (3.37)$$

In addition, there is a method to improve the convergence rate of the algorithm when the environment upon which the algorithm operates is wide-sense-stationary. This involves a normalization of the coefficient step size  $\mu$  with the average signal power of the reference signal for each block. More specifically, the constant  $\mu$  will change as follows:

$$\mu_i = \frac{a}{\mathbf{P}_i}, \text{ with } i = 0, 1, \dots, 2M-1 \quad (3.38)$$

where  $a$  is a constant and  $\mathbf{P}_i$  the average power in a specific frequency bin. As a consequence, the  $M$ -by-1  $\mathbf{D}[k]$  vector is created, which is described as follows:

$$\mathbf{D}[k] = \left[ \mathbf{P}_0^{-1}[k] \quad \mathbf{P}_1^{-1}[k] \quad \dots \quad \mathbf{P}_{2M-1}^{-1}[k] \right]^T \quad (3.39)$$

and the Eq. (3.36) will vary accordingly:

$$\phi[k] = \text{first } M \text{ elements of } \text{IFFT}[\mathbf{D}[k] \odot \mathbf{U}^*[k] \odot \mathbf{E}[k]]. \quad (3.40)$$

Also, the term  $\mu$  of Eq. (3.37) will be replaced by the term  $a$  of Eq. (3.38), which is a constant chosen by the user. Fig. 3.4 is a schematic representation of the algorithm, as analysed previously.

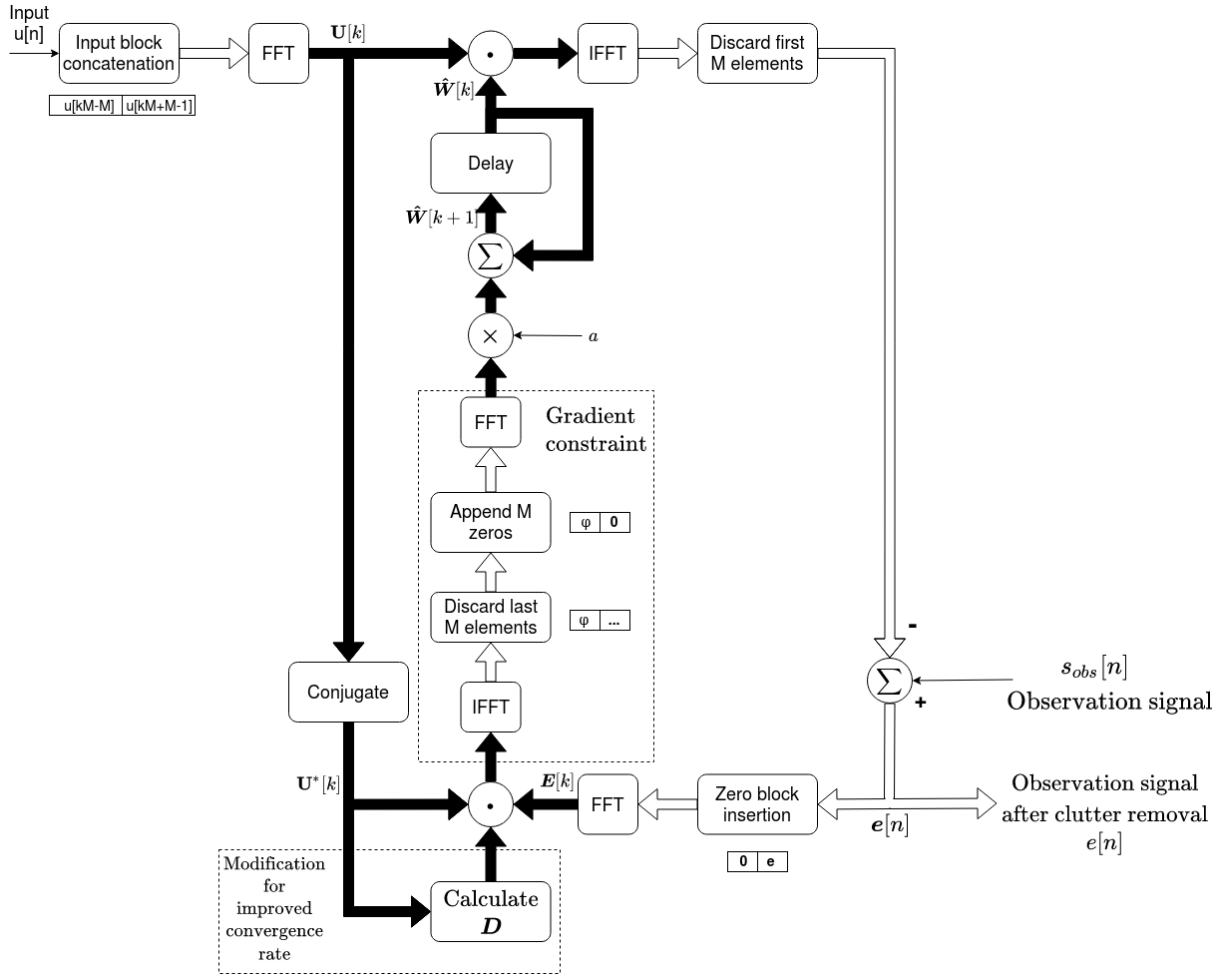


Figure 3.4: A schematic representation of the FBNLMS algorithm.

The black arrows mean that the operation took place in the frequency-domain and the white arrows in the time-domain.

# Chapter 4

## ARD Surface plot

### 4.1 Cross-ambiguity function

By now, the data preprocessing and clutter removal stages have taken place. The outcome will be consisting of the targets' echoes  $s_{tar}[n]$ , given that they exist, and noise. Therefore, the information of the  $s_{tar}[n]$  must be used to detect the targets.

The equation following is the cross-ambiguity function:

$$|\psi(\tau, f)| = \left| \sum_{n=0}^{C-1} s_{tar}[n] s_r^*[n - \tau] \exp\left(\frac{j2\pi f n}{F_s}\right) \right|, \quad (4.1)$$

where the target's reflection  $s_{tar}[n]$  is correlated with the reference signal  $s_r[n]$ , which is delayed in time by a constant  $\tau$ .  $F_s$  is the sampling rate and  $C$  the CPI. If  $\psi(\tau, f)$  has a large value for a specific set of  $\tau, f$  compared to the neighbouring calculations, then a bright spot will appear in this position in the two-dimensional plot of range-Doppler.

A major difference between noise and targets is that targets seem to linearly change their Doppler and range measurement or at least one of them, in comparison to noise that appears in random positions and then disappears, without any continuity in the neighbouring cells.

CPI or  $C$  must be chosen carefully in Eq. (4.1), since it will determine the Doppler resolution, or the ability to detect signals' small frequency changes. In our case, CPI is equal to 262144 complex samples. Each complex sample is captured with a sampling frequency of 2.4MHz. Then, it is decimated by a factor of 10, to restrict the sampling frequency close to the bandwidth of the chosen FM channel. Therefore, each frame contains samples captured over a period equal to:

$$CPI = \frac{262144 S}{240 \text{ kS/sec}} = 1.09 \text{ sec}. \quad (4.2)$$

This means that for every 1.09sec of capturing samples with both antennas, one ARD surface frame is produced.

The Doppler resolution (D) is associated to the CPI by the following equation:

$$D = \frac{1}{CPI} = \frac{1}{1.09} = 0.92 \text{ Hz.} \quad (4.3)$$

Therefore, signals with frequency difference 0.92 Hz can be separated. With a larger CPI, better Doppler resolution can be achieved. The trade-off in increasing the CPI is that it will cause computations to be consisting of larger vectors and matrices, which would increase the computational cost.

Calculating the range-Doppler of Eq. (4.1) is computationally expensive. Therefore, the approximate method of calculating the CAF using "Fine Mode" is used. This is explained in [16] and [7] and it exploits the Fast Fourier Transform to speed up the process.

The cross-ambiguity  $C$  term of the CPI, is separated into two arbitrary numbers  $Q$  and  $V$ , maintaining that  $C = Q * V$ , so that:

$$\psi(\tau, f) = \sum_{k=0}^{Q-1} \left[ \sum_{l=0}^{V-1} s_{tar}[l + kQ] s_r^*[l + kQ - \tau] \exp\left(\frac{j2\pi l f}{F_s}\right) \right] \exp\left(\frac{j2\pi k Q f}{F_s}\right). \quad (4.4)$$

In Eq. (4.4), if  $f_{max} V \ll F_s$ , then the term  $\exp\left(\frac{j2\pi l f}{F_s}\right) \approx 1$  and is removed. Then, what we are left with is:

$$\psi(\tau, f) = \sum_{k=0}^{Q-1} \left[ \sum_{l=0}^{V-1} s_{tar}[l + kQ] s_r^*[l + kQ - \tau] \right] \exp\left(\frac{j2\pi k Q f}{F_s}\right), \quad (4.5)$$

and by setting:

$$g(k, \tau) = \sum_{l=0}^{V-1} s_{tar}[l + kQ] s_r^*[l + kQ - \tau], \quad (4.6)$$

the cross-ambiguity function can be approximated as follows:

$$\psi(\tau, f) \approx \sum_{k=0}^{Q-1} g(k, \tau) \exp\left(\frac{j2\pi k Q f}{F_s}\right). \quad (4.7)$$

In Eq. (4.7) we observe that the cross-ambiguity has turned into the DTFT of  $g(k, \tau)$ . The DTFT is implemented in computers by the Discrete Fourier Transform(DFT) which is calculating the Fourier Transform between  $-F_s/2$  and  $F_s/2$ . This means that most of the computations will be useless, since the bandwidth of

the signal is relatively large ( $\approx 240kHz$ ), compared to the frequency shifts that we search for ( $\approx 500Hz$ ). Therefore, a decimation of the cross-correlation product  $g(k, \tau)$  is used, leading to a significant reduction of the overall computation time.

Prior to the decimation an anti-alias filter is used to restrict the bandwidth of the signal to satisfy the Nyquist-Shannon sampling theorem. The two methods used, Fine-Mode and Fine-Mode with generic filter are described in [16]. To compute the DFT the Fast Fourier Transform (FFT) is used.

The process described above is described schematically in Fig. 4.1:

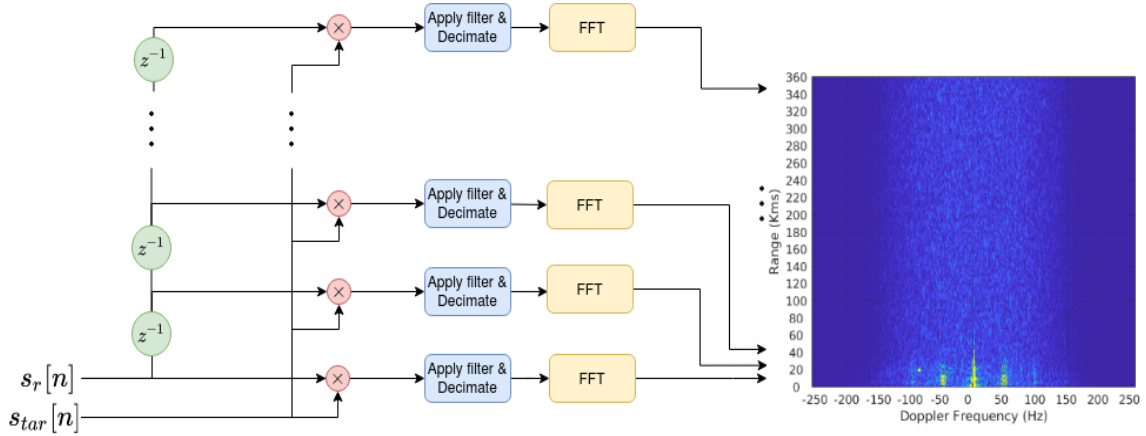


Figure 4.1: "Fine mode" cross-ambiguity computation for faster calculation of  $\psi(\tau, f)$ .

## 4.2 Constant False Alarm Rate

CFAR (Constant False Alarm Rate) [6], [7] is a method of separating target echoes from a background of noise and remaining clutter and it is used right after the ARD surface calculation.

The Cell-Averaging CFAR (CA-CFAR) algorithm is producing multiple 2D frames of the same size as the ARD plots. The values of this matrix are computed by setting the Cell's Under Test (CUT) value equal to the reference cells' mean value, ignoring the guard cells. The kernel used to filter the image is shown in Fig. 4.2.

The guard cells are ignored to ensure that the CUT's value is substituted by a value close to the noise's mean value. In the opposite case, the noise part could contain scattering information and thus have a larger value, which would deteriorate the performance of the CFAR algorithm.

Then, each cell of the cross-ambiguity ARD surface is divided with the filtered CFAR surface. This lowers the level of noise in the image and therefore, enhances

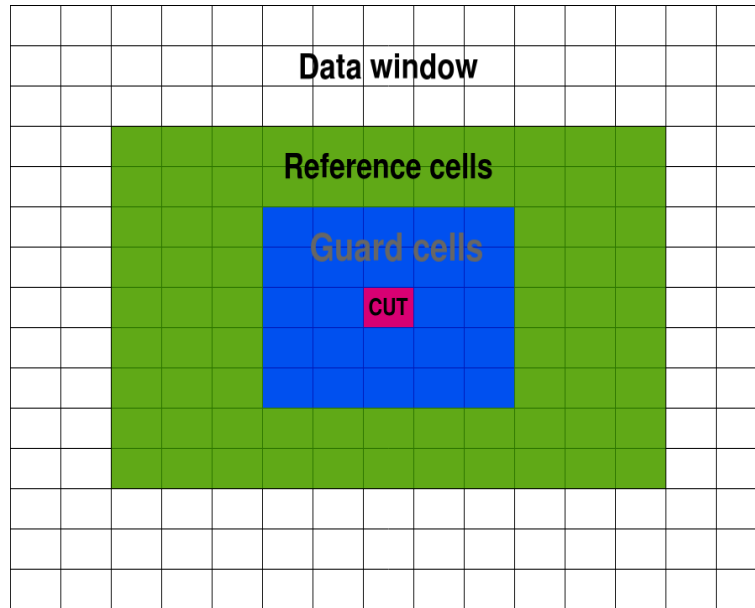


Figure 4.2: CFAR kernel: Cell Under Test(CUT) with red, Guard cells with blue, Reference cells with green and the rest of the frame in white(Data window).

the target's amplitude in relevance to the noise floor. In the resulting image, only the cells' with value above a threshold are shown, otherwise they are filtered out and set to a minimal value. The threshold is empirically set. In our case, a CAF bin should be 5.4db greater than the CA-CFAR corresponding bin to be avoid being minimized.

In the next pictures, the effect of the CA-CFAR algorithm is displayed. Marked with a red circle is the target. It is obvious that the filtered ARD surface is cleaned from noise and the remaining clutter. Hence, one can observe the target in the filtered image with more ease.

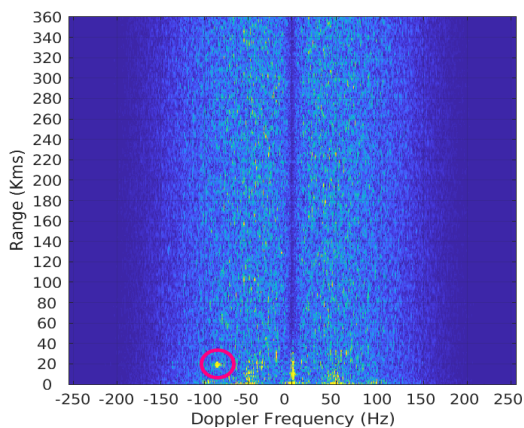


Figure 4.3: Without CFAR.

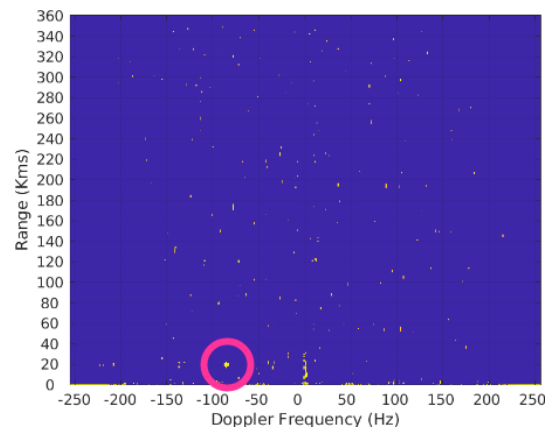


Figure 4.4: With CA-CFAR.

# Chapter 5

## Experimental results

### 5.1 Adaptive Filters' performance

All the adaptive filter algorithms, with the exception of the LMS, are implemented for the PR and an evaluation of their performance will be presented. All the results are by using experimental data.

First, the algorithms were evaluated in terms of the time they need to remove the clutter over one CPI of length 262144 samples. Also, the clutter suppression they achieved will be evaluated.

The Least-Squares algorithm was chosen to operate over a block size equal to the CPI. Also, the LS removed the clutter only from the 0 Doppler frequency. For additional clutter suppression, it could, also, be performed in neighbouring Doppler bins at the expense of increased processing time. In addition, the algorithms required some tuning of their parameters to operate optimally. This was a difficult task since the combinations of the parameter values are unlimited. For simplicity purposes, the BNLMS and FBNLMS the filter's length  $M$  is chosen equal to the block length  $L$ . Table 5.1 contains the parameters for each algorithm that were found to work sufficiently good for each algorithm. The BNLMS will be discarded, since it has the same outcome with the FBNLMS, but with increased processing time.

Table 5.1: Parameters of each algorithm.

Filter	$L$	$M$	$\mu$	b	a
LS	–	128	–	–	–
NLMS	–	1024	0.1	$2 \times 10^{-3}$	–
BNLMS	1024	1024	0.6	$2 \times 10^{-3}$	–
FBNLMS	1024	1024	–	–	0.1

The filter taps of the LS filter are set to 128. This is because inverting the matrix  $(\mathbf{X}^H \mathbf{X})$  and, thus, computing the filter coefficients has complexity  $O(n^{2.3})$  to  $O(n^3)$ . As a result, for a large  $(\mathbf{X}^H \mathbf{X})$  the algorithm is too slow. Hence, there were the options of reducing the CPI or reducing the filter taps. In [9], the first option was

chosen. In this work, the filter taps of the LS filter were reduced.

The average processing time to perform the clutter removal in one CPI is shown in the following table:

Table 5.2: Clutter removal of various algorithms in seconds.

LS	NLMS	BNLMS	FBNLMS
2.2s	6.3s	4.8s	0.7s

In order to construct a real-time PR, the best choice of Adaptive filter is the FBNLMS, since it is the only algorithm that can perform its task in less time than the CPI ( $0.70sec < 1.09sec$ ). The LS filter is closer to the CPI time than NLMS. This is without much optimization, meaning that it could potentially be used for a real-time PR.

The DSI suppression of each algorithm should also be evaluated, by measuring the noise floor reduction of each algorithm. For simplicity purposes, since BNLMS and FBNLMS are the same algorithms, only the FBNLMS will be evaluated in terms of clutter suppression. The metrics used were provided by [13].

The equation to measure the noise floor ratio is:

$$R_{NF} = \frac{\sum_{\tau \in T, f \in F} |\psi(\tau, f, s_f)|^2}{\sum_{\tau \in T, f \in F} |\psi(\tau, f, s_o)|^2}, \quad (5.1)$$

with  $T$  the time delays,  $F$  the frequencies taken into consideration and  $\psi$  the cross-ambiguity function, which is given as follows:

$$\psi(\tau, f, s) = \sum_{n=0}^{C-1} s[n]s_r^*[n - \tau] \exp\left(\frac{j2\pi n f}{F_s}\right), \quad (5.2)$$

where  $s$  is any signal chosen. When the measurement of  $\psi$  is over the unfiltered observation signal, it is  $\psi(\tau, f, s_o)$  and when it is over the filtered one, it is  $\psi(\tau, f, s_f)$ .

The results of each filter noise floor reduction will be measured in dB over the zero Doppler-zero Range bin of the corresponding unfiltered cross-ambiguity frame. Also, the CFAR step is neglected for these measurements to avoid distortion of the results. The results are shown in Table 5.3.

Table 5.3 shows that the NLMS has the best performance in lowering the noise floor level. As a result, it is the best choice when clutter removing accuracy is the case. The FBNLMS did not lower the noise floor as well.

Table 5.3: Comparison of the noise floor reduction of various algorithms, relative to the (0,0) unfiltered ARD value (dB).

Algorithm	Noise Floor (dB)
–	-46.2
Least Squares	-79.4
NLMS	-84.3
FBNLMS	-78.1

The clutter reduction can also be observed in real data. The following frames are over the same CPI. The four frames represent different scenarios. At first, there is a picture without clutter removal. Then, the pictures are after the DSI suppression process with the Least-Squares, the NLMS and the FBNLMS filter. The colorbar which is on the side of each figure is representing the floor and ceil of the amplitude in decibels, relative to the zero-Doppler and zero-range bin of the unfiltered ARD surface.

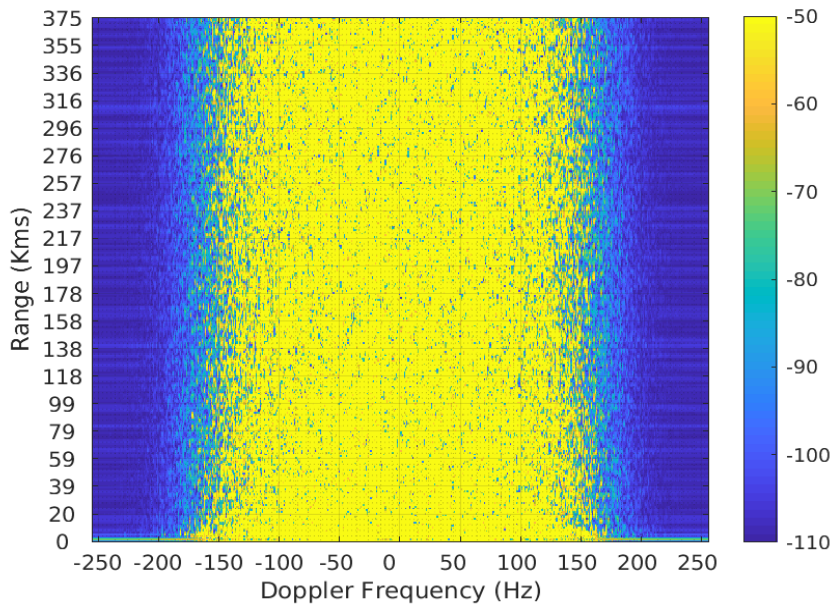


Figure 5.1: Unfiltered picture.

In Fig. 5.1, due to the increased noise floor, it is impossible to detect the target. In the next figures the target is marked with a red circle.

The NLMS algorithm achieves the best performance in terms of clutter removal. As a result, the NLMS has the lowest overall noise floor value. This can be seen in Fig. 5.3. Also, it has no effect on the amplitude of the target's echo. The FBNLMS

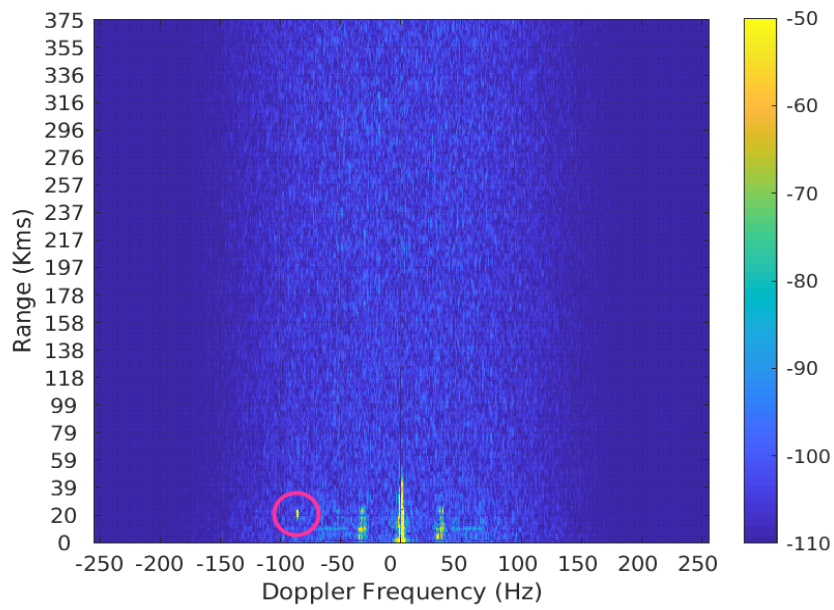


Figure 5.2: Least-Squares filter.

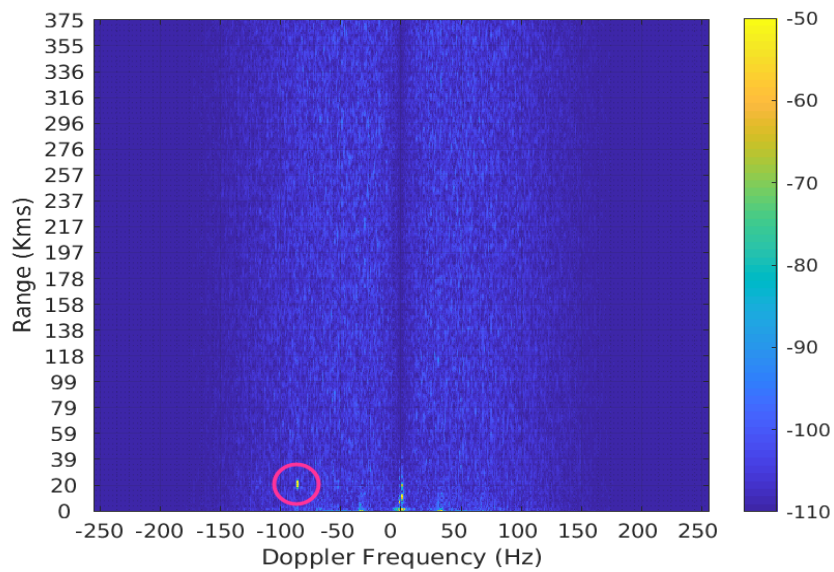


Figure 5.3: NLMS filter.

has the poorest performance as expected, while the Least-Squares is slightly better but still inferior to NLMS.

Given the above results, when real-time operation is not requested, the best DSI suppression is achieved by the NLMS algorithm. For real-time application the best choice is the FBNLMS. Least-Squares could be used as a compromise between speed

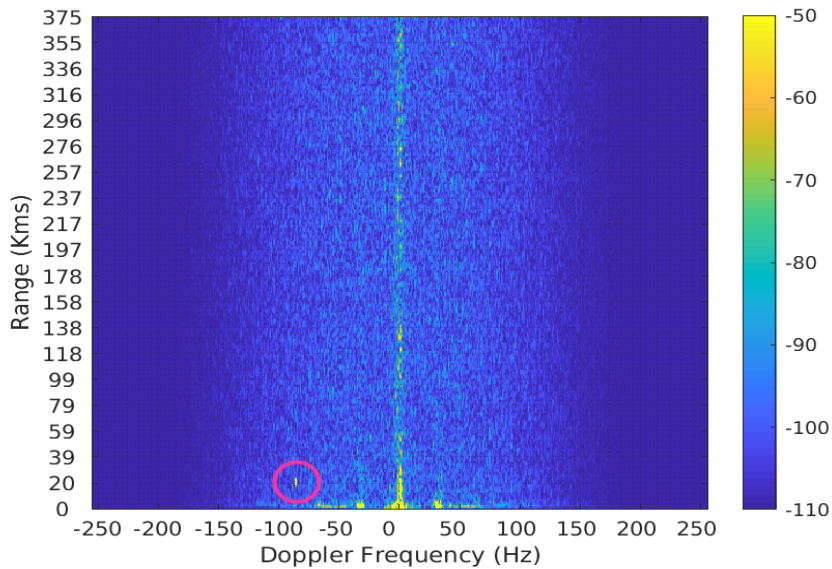


Figure 5.4: FBNLMS filter.

and DSI suppression accuracy and an optimized, paralleled version could also be used for real-time operation.

The FBNLMS has higher noise floor, compared to LS, between the ranges of  $-100$  to  $100$  Hz in frequency and  $0$  to  $375$  km in bistatic range. Outside of this area, the noise floor has similar values. Therefore, it is shown that, as stated in [9], given that the FBNLMS algorithm is computationally more efficient, it could be a better choice for fast moving targets. The LS filter will work more accurately for slow moving targets.

## 5.2 Range-Doppler accuracy

The accuracy of the system was measured by using a flight tracking application. More specifically, the flight OAL5SA from the Ioannis Daksalogiannis, Chania to Eleftherios Venizelos, Athens was tracked. The plane is an Airbus A320. In Fig. 5.5, the application's calculation of the coordinates, speed and elevation of the plane is shown:

The positions mentioned in Fig. 5.5, are marked in Google Earth as shown in Fig. 5.6.

The coordinates given by the app have a yellow placemark. For each placemark, the Doppler frequency and bistatic range is calculated.

Fig. 5.7 is containing the bistatic radar geometry, according to [1]. The target's

Time (EEST)	Latitude	Longitude	Course	kts	km/h	meters
<b>Tue 07:34:15 PM Departure (CHQ / LGSA) @ Tuesday 07:34:15 PM EEST</b>						
Tue 07:34:15 PM	35.5423	24.1168	← 293°	163	303	556
Tue 07:34:34 PM	35.5476	24.1011	← 293°	168	311	754
Tue 07:34:50 PM	35.5529	24.0853	← 293°	190	352	930
Tue 07:35:10 PM	35.5641	24.0666	↖ 326°	214	396	1,067
Tue 07:35:28 PM	35.5808	24.0628	↑ 4°	213	394	1,311
Tue 07:35:44 PM	35.5964	24.0650	↑ 8°	228	422	1,547
Tue 07:36:01 PM	35.6156	24.0681	↑ 8°	254	470	1,775
Tue 07:36:19 PM	35.6377	24.0659	↑ 348°	267	494	2,073
Tue 07:36:38 PM	35.6591	24.0550	↑ 348°	263	488	2,469
Tue 07:37:08 PM	35.6976	24.0552	↑ 2°	295	546	2,865

Figure 5.5: Tracking application information.

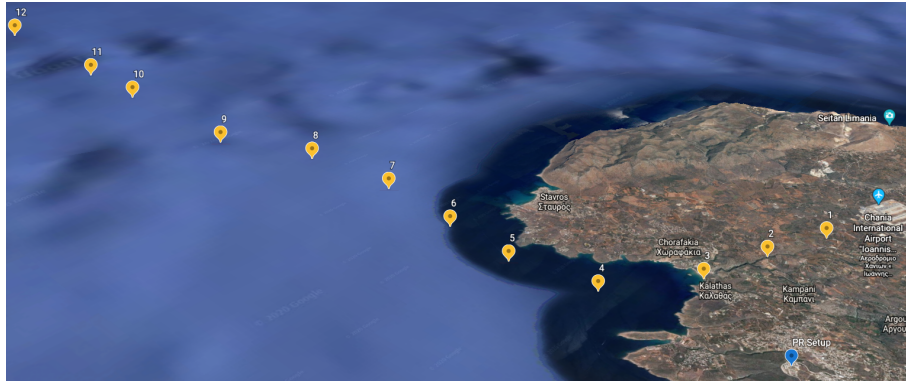


Figure 5.6: Coordinates of the plane during flight OAL5SA, according to tracking app.

position will be on ellipses, with the PR setup and the FM transmitter being the two focal points. The angle subtended at the target by the PR setup and FM transmitter is called bistatic angle  $\beta$ . The angle between the velocity vector of the target and the bisector of the angle  $\beta$  is denoted as  $\delta$ .  $R_R$  is the distance of the PR setup with the target,  $R_T$  is the distance of the FM transmitter with the target and  $L$  is the baseline connecting transmitter and receiver.

According to [1], the Doppler frequency is given as follows:

$$f_D = \frac{2v}{\lambda} \cos \delta \cos (\beta/2), \quad (5.3)$$

where  $v$  is the target velocity,  $\beta$  is the bistatic angle and  $\delta$  the angle between the target's velocity and the bisector of the bistatic angle.

The following graph is showing the comparison between the theoretic Doppler measurements from the map and the corresponding radar measurements.

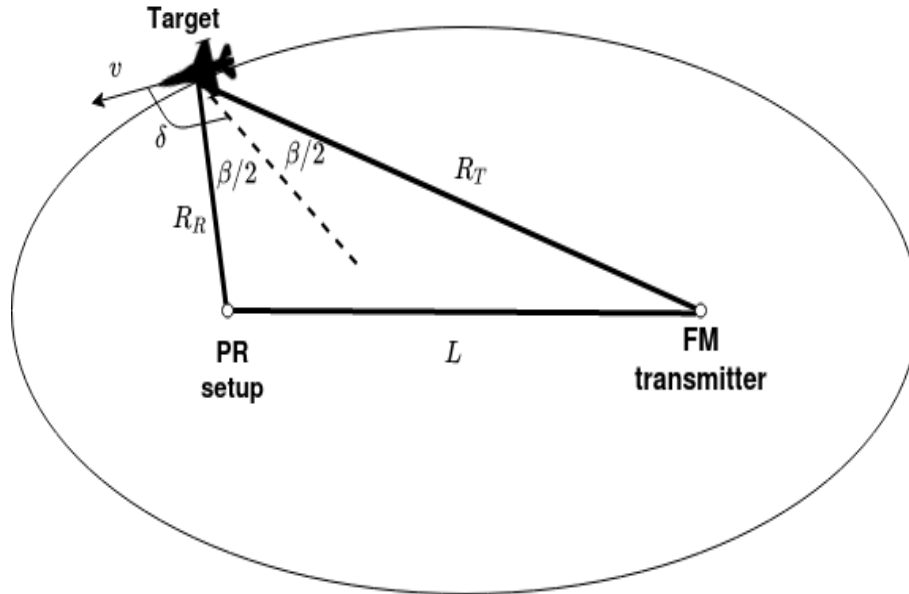


Figure 5.7: The bistatic radar geometry.

The Doppler measurement, as seen in Fig. 5.8, has an average error of  $\pm 7$  Hz and a maximum error of 15 Hz, through all the measurements. This error resulted during the turn of the plane, landmark 4 in Fig. 5.6. As a result, it could be due to error in the direction of the plane. The course of the plane is given from the tracking app, as shown in Fig. 5.5, but it could be not completely accurate, especially during a turn.

The range in the ARD surface is displaying the distance  $R_T + R_R - L$ . The  $L$  term is the baseline, which is a constant (7.3 km to the FM Station of Malaxa). For the range measurements, the elevation of the plane in each frame, the elevation of the PR setup (142 m) and the FM transmitter (1921 m) were taken into consideration. The results are shown in Fig. 5.9.

The range calculation has an average error of 2795 metres. The maximum error is 5620 metres at the second measurement. As the plane flies away, the range measurement becomes more accurate. This is possibly because when the plane is close, its depiction in the ARD surface is broader due to the increased scattering taking place. When the bistatic range is small, even small misjudgements in the radar's range measurement can cause great error.

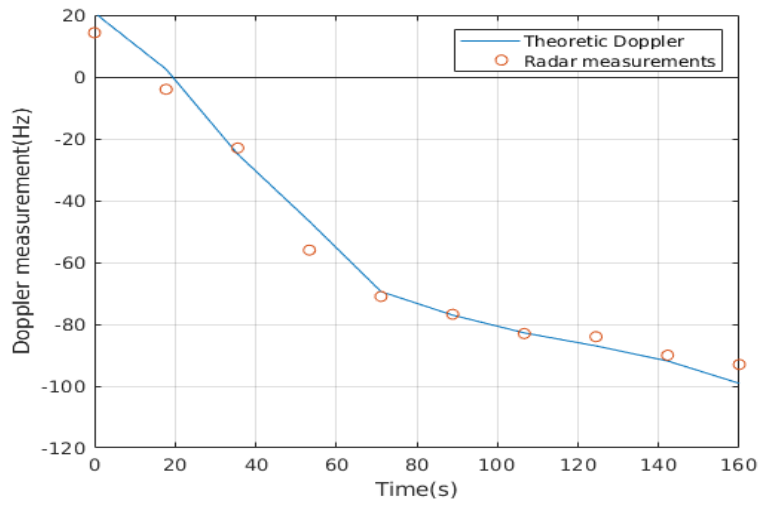


Figure 5.8: Doppler measurements of the radar versus the theoretical.

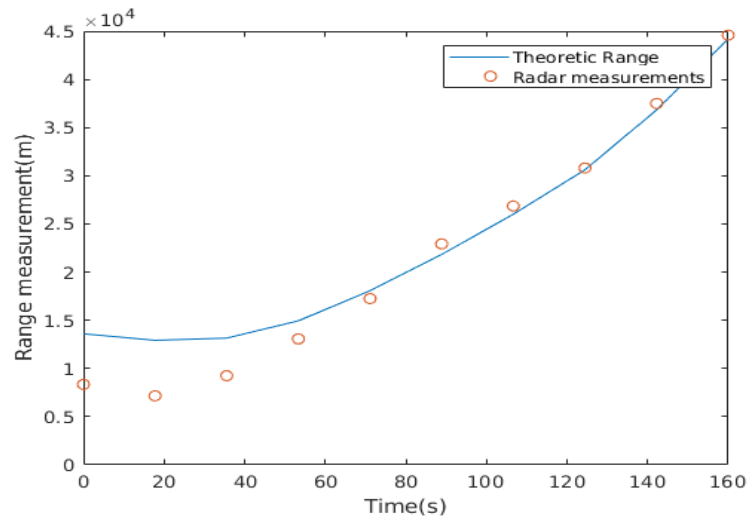


Figure 5.9: Range measurements of the radar versus the theoretical.

# Chapter 6

## Conclusions

Concluding, this thesis contains a fully operational FM passive radar, along with a detailed explanation of its components. Various adaptive filtering algorithms were implemented. Their DSI suppression accuracy and time efficiency was compared. NLMS showed to be the best algorithm in terms of reducing the overall noise floor but did not satisfy accordingly in terms of time efficiency. FBNLMS was the fastest algorithm, but the overall noise floor did not lower down as much as NLMS, with an overall noise floor difference of 6.2 dB. Nevertheless, due to its effectiveness, it could be used for real time applications where time efficiency is necessary. Least-Squares filter is the trade-off between time efficiency and noise floor reduction. It is preferred for slow moving targets over FBNLMS, while FBNLMS is preferred for fast moving targets over LS. The accuracy of the passive radar was also presented, in terms of both Doppler and bistatic range measuring.

To continue this work, we want to add a direction of arrival estimation, using phase interferometry. Also, the addition of a Low Noise Amplifier along with a Band-pass filter could increase drastically the range from 25 kms that it is now. Also, the development of a tracker, i.e. Kalman filter would also improve the radar's operation. The use of multiple transmitters and channels could help localizing the target. Additionally, other illuminators of opportunity will be examined.

# Bibliography

- [1] H. Griffiths and C. Baker, *An Introduction to Passive Radar*. Artech House, 2017.
- [2] H. Griffiths and N. Willis, “Klein Heidelberg: The First Modern Bistatic Radar System,” *IEEE Trans. Aerosp. Electron. Syst.*, vol. 46, pp. 1571 – 1588, Nov. 2010.
- [3] H. Kuschel and D. O’Hagan, “Passive radar from history to future,” in *11-th International Radar Symposium*, Aug. 2010, pp. 1–4.
- [4] J. Vierinen. [Online]. Available: <https://hackaday.com/2015/06/05/building-your-own-sdr-based-passive-radar-on-a-shoestring>
- [5] J. Sahr and F. Lind, “The Manastash Ridge radar: A passive bistatic radar for upper atmospheric radio science,” *Radio Science*, vol. 32, pp. 2345–2358, Nov. 1997.
- [6] P. Howland, D. Maksimiuk, and G. Reitsma, “FM radio based bistatic radar,” *Radar, Sonar and Navigation, IEE Proceedings*, vol. 152, pp. 107 – 115, Jul. 2005.
- [7] M. Manning. [Online]. Available: <https://dopplerfish.com/passive-radar/>
- [8] K6STI, “Small five-element yagi.” [Online]. Available: <http://ham-radio.com/k6sti/five.htm>
- [9] J. L. Garry, G. E. Smith, and C. J. Baker, “Direct signal suppression schemes for passive radar,” in *2015 Signal Processing Symposium (SPSymposium)*, Jun. 2015, pp. 1–5.
- [10] S. Haykin, *Adaptive Filter Theory : International Edition, 5th Edition*, 5th ed. Pearson, 2014.
- [11] B. Widrow and M. E. Hoff, “Adaptive switching circuits,” in *1960 IRE WESCON Convention Record, Part 4*. New York: IRE, 1960, pp. 96–104.

- 
- [12] G. N. Karystinos, *Notes on Statistical Signal Processing for Telecommunications*. Technical University of Crete.
- [13] T. Peto, L. Dudas, and R. Seller, “DVB-T based passive radar,” *2014 24th International Conference Radioelektronika*, pp. 1–4, Apr. 2014.
- [14] Y. Zhao, Y. Zhao, X. Lu, and M. Xiang, “Block NLMS cancellation algorithm and its real-time implementation for passive radar,” *IET Conference Publications*, vol. 2013, pp. 1–5, Jan. 2013.
- [15] E. Ferrara, “Fast implementations of lms adaptive filters,” *IEEE Transactions on Acoustics, Speech, and Signal Processing*, vol. 28, no. 4, pp. 474–475, Aug. 1980.
- [16] C. L. Yatrakis, “Computing the Cross Ambiguity Function - A Review,” Master’s thesis, Binghamton University, State University of New York, 2005.